The Effect of Defects on the Fatigue Crack Initiation Process in Two P/M Superalloys: Part I. Fatigue Origins

J. M. HYZAK and I. M. BERNSTEIN

Two high strength P/M nickel-base superalloys, AF-115 and AF2-1DA, with different defect populations, were tested to determine the effect of preexisting defects on the fatigue crack initiation process. Strain controlled continuous cycle fatigue tests were performed at room and at elevated temperature; these were followed by fractographic examination to characterize both the location and character of the fatigue origins. In most cases, particularly at elevated temperature, the initiation process was associated with a large pre-existing defect, either a pore or a nonmetallic inclusion. There was also a change in the location of the crack that caused failure as the strain range varied: at high strain ranges initiation occurred at or near the specimen's surface, while at the lower strain ranges the failure originated in the specimen's interior. The initiation mode for both alloys at room temperature was different than at elevated temperature. At room temperature, Stage I crystallographic cracking at or near the surface dominated the process in all strain range regimes. This difference was attributed, in part, to the differences in deformation mode for nickel-base superalloys at room and elevated temperature.

I. INTRODUCTION

IT has been well established in the literature that microstructural defects significantly affect fatigue crack initiation.[1-4] In fact, it has generally been accepted that in engineering alloys crack initiation invariably occurs at some preexisting defect.[5,6] However, few experimental studies have been performed to determine specifically the relative influences of defect size, shape, and population on the fatigue process. It was therefore the purpose of this investigation to examine the effect of such defect characteristics on crack initiation and the early crack growth behavior of two high strength nickel-base superalloys, AF-115 and AF2-1DA. Both alloys were produced by powder metallurgy (P/M) techniques and contained contrasting populations of preexisting pores and nonmetallic inclusions. The testing conditions included a span of temperatures and strain ranges in order to determine the effect of defects in variable regimes where deformation behavior differed.

This study is reported in two parts; in the first paper the details of the crack initiation processes for both alloys over a range of test conditions are reported. These include the identification of the fatigue origins and a description of the early crack growth morphology in the different testing regimes. In the accompanying paper,[7] these data are analyzed along with the results of some additional testing, in order to establish the behavior patterns and the general effect of defect size, shape, and population on the fatigue process of these and similar alloys.

II. MATERIALS

A. *Processing*

The composition of the AF-115 alloy used in this study is shown in Table 1. Powders of this composition were produced by an argon atomization process and were subsequently processed in either of two ways: hot isostatically pressed (HIPed) and heat treated; and HIPed, forged, and heat treated. Specimens from material of both conditions were tested in this program. The HIP parameters were 1190 °C for two hours at 100 MPa, and the forging conditions were 1120 to 1150 °C at a press head velocity of 25 to 10 cm per minute using preheated die blocks. A total reduction of approximately 50 pct was accomplished in the forging step. All material was subsequently solution heat treated at 1190 °C for four hours followed by an aging treatment at 775 °C for 16 hours.

The AF2-1DA powder whose composition is given in Table 2 was also produced using the argon atomization process. The powder was compacted, extruded, and finally superplastically forged, the latter at 1105 °C. The pancakes were then solution treated at 1210 °C for two hours, stabilized at 1121 °C for two hours, and finally aged at 705 °C

Table 1. AF-115 Chemical Analysis; Wt Pct

Element	
C	.155
Mn	<.01
Si	.03
P	<.005
S	.002
Cr	10.20
Ni	Bal.
Mo	2.62
Co	14.95
Ti	3.90
Al	3.85
Cb	1.62
W	5.62
B	.023
Hf	2.02
Zr	.045
O	.0044
N	.001

J. M. HYZAK, formerly with Metals and Ceramics Division, Air Force Materials Laboratory, Wright-Patterson AFB, OH, is now Member of the Technical Staff, Sandia National Laboratories, Livermore, CA 94550. I. M. BERNSTEIN is Professor, Department of Metallurgical Engineering and Materials Science, Carnegie-Mellon University, Pittsburgh, PA 15213.

Manuscript submitted March 6, 1981.

ISSN 0360-2133/82/0111-0033$00.75/0

Table 2. Chemical Composition AF2-1DA Wt Pct

Cr	12.22	Zr	.084
Ti	2.89	Si	<0.1
Co	10.10	Fe	<0.1
W	5.70	B	.016
Al	4.70	C	.31
Mo	3.00	S	.007
Ta	1.90	P	< .002
Mn	<0.1	O_2	65 PPM

Balance – Nickel

for 12 hours and 816 °C for eight hours. These parameters had been previously developed in order to optimize the combination of strength and ductility for both alloys.

B. *Microstructure*

The microstructures of the HIP and HIP + forged conditions of AF-115 were similar, differing only in final grain size. The AF-115 microstructure was dominated by three sizes of γ' precipitate, two of which are resolved in Figure 1. The irregular-shaped unsolutionized γ' were located along grain boundaries and were approximately 3 to 10 μm along their major axes, while the cuboidal cooling γ' within the grains were approximately 0.25 μm on edge. The ultra-fine aging γ' were more spherical and measured 0.02 to 0.04 μm in diameter. The average grain diameter of the as-HIP AF-115 was 30 μm, while the HIP + forged grain diameter was approximately 19 μm.

The AF2-1DA microstructure also had three sizes of γ' precipitate with the larger two resolved in Figure 2. The irregular shaped primary γ' (1 to 3 μm) decorated the grain boundaries while cuboidal cooling γ' (0.25 μm) and fine aging γ' (0.06 to 0.08 μm) were contained within the grains. The grain diameter was approximately 200 μm.

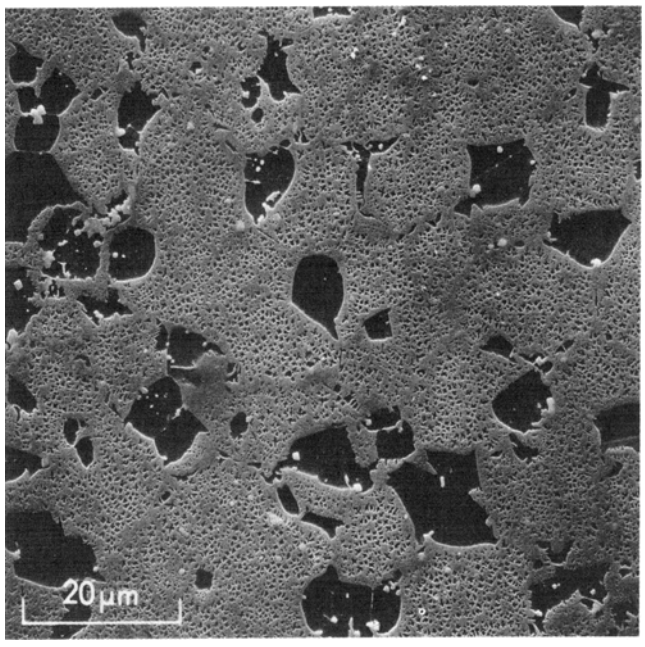

Fig. 1—SEM micrograph of the AF-115 microstructure showing the large unsolutioned γ' and the smaller cooling γ'.

Fig. 2—SEM micrograph of the AF2-1DA microstructure showing the morphology of the grain boundary γ' and cooling γ', as well as the carbide distribution.

C. *Defects*

There were three distinct defect types found in this particular heat of AF-115 alloy: pores, tramp nonmetallic inclusions, and hafnium oxide inclusions. The pores, the most populous of the defects, measured up to 130 μm in diameter and were a by-product of the argon atomization process. The level of porosity was quantitatively determined by a thermal induced porosity (TIP) test; the change in density due to the porosity was 0.42 pct. While this porosity level is probably too high to allow the alloy heat to be used for many applications, it did provide an ideal material with which to study the effect of spherical defects.

The next most prevalent defects were the nonmetallic inclusions such as tramp ceramic pieces of equipment liners with a population much less than that of the pores. The inclusions size ranged up to 100 μm in length, and their shape varied from spherical to elliptical. The density of pores and inclusions in AF-115 is shown in a representative micrograph in Figure 3a.

The least populous defects in this heat of AF-115 were plate-like particles identified with the microprobe as hafnium oxide inclusions (probably HfO_2). These particles were up to 125 μm in diameter with a thickness of only 5 μm.

Although the AF2-1DA powder was also produced by the argon atomization technique, the processing of this heat of powder was such that there was no significant level of porosity. Since there was no hafnium in the AF2-1DA, there were also no HfO_2 inclusions in the material. The only defects were nonmetallic inclusions similar in size and population to those in the AF-115 alloy. A representative micrograph of the inclusion density in AF2-1DA is shown in Figure 3b.

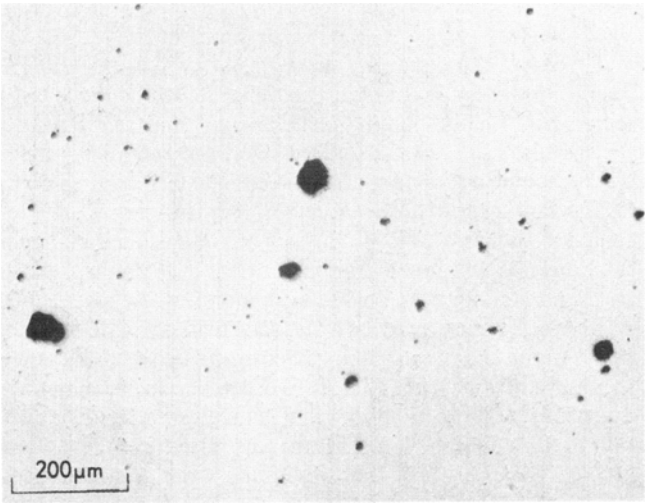

(*a*)

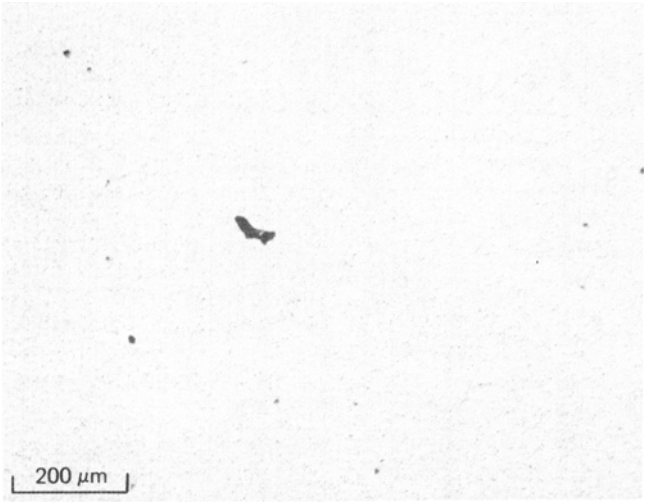

(*b*)

Fig. 3 — SEM micrographs showing defect distributions in (*a*) AF-115 and (*b*) AF2-1DA.

D. *Tensile Properties*

The tensile properties of both alloys at 760 °C are summarized in Table 3. The HIP + forged condition of AF-115 had a slightly higher average yield strength than the as-HIP condition, but they were both superior to the strength of the AF2-1DA alloy. As expected, the AF2-1DA microstructure showed greater ductility because of its relative cleanliness and lower strength.

III. EXPERIMENTAL PROCEDURE

Uniform section specimens were tested in total strain control using a servohydraulic closed-loop fatigue system and an axial extensometer. Standard specimen preparation techniques were used, including low stress grinding and mechanical polishing of the gage section; specimen dimensions are shown in Figure 4.

Specimens were tested at 760 °C, 649 °C, and 22 °C using a sawtooth waveform strain path at frequencies of 20 cycles per minute (cpm) and 0.2 cpm. 760 °C was the maximum temperature at which both alloys maintained their high strength. Specimens were tested at a strain ratio, A, of +1 where:

$$A \equiv \frac{\text{Alt. Strain}}{\text{Mean Strain}}. \qquad [1]$$

Tests were run until specimen fracture.

Scanning electron microscopy (SEM) was utilized as the major analytical tool for this effort. The SEM fractographic study centered on identifying both the location and character of the fatigue origin and the morphology of the early crack growth. The crack that was identified as being responsible for failure was termed the "dominant" crack.

Failed specimens were also sectioned axially, mounted and polished, and examined. "Secondary" cracks, defined as those cracks that initiated independent of the dominant crack but were not responsible for failure, were identified and then studied using optical microscopy, the SEM, and, in some cases, standard two-stage replica transmission electron microscope (TEM) techniques.

IV. RESULTS AND DISCUSSION

A. *Fatigue Behavior*

The fatigue data for the AF-115 and AF2-1DA alloys are presented in Figures 5 and 6, respectively. Since the microstructures and mechanical behavior of the HIP and HIP + forged conditions of AF-115 are very similar, they are both treated as one population in this analysis. However, a more detailed treatment of the fatigue results including tabulation of the data is presented elsewhere.[8]

Table 3. Tensile Properties, 760 °C

Spec.	0.2 pct Y. S., MPa (ksi)		UTS, MPa (ksi)		Elong. (pct)	R_a (pct)
AF-115-HIP						
2-19	989	(143.5)	1156	(167.7)	8.3	11.6
7-19	1013	(146.9)	1196	(173.4)	7.6	12.9
9-20	1051	(152.5)	1192	(172.9)	8.9	9.5
AF-115-HIP + Forge						
5-33	1040	(150.9)	1132	(164.2)	8.0	13.1
5-35	1041	(151.0)	1164	(168.8)	10.0	12.8
AF2-1DA						
B2-4	909	(131.8)	958	(138.9)	–	17.9
B2-5	898	(130.3)	964	(139.8)	–	17.5

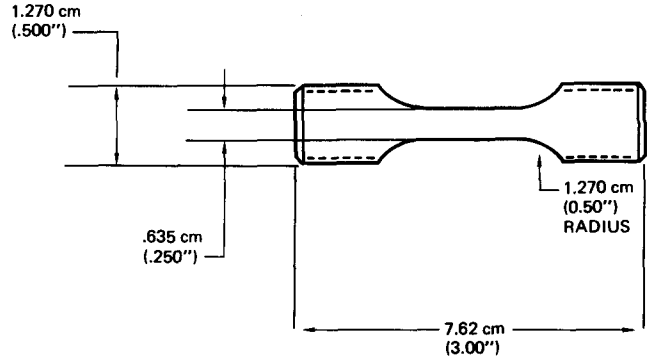

Fig. 4—Uniform section smooth bar fatigue specimen.

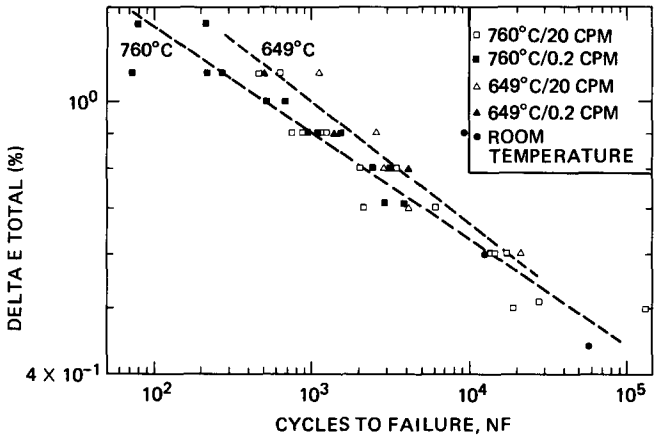

Fig. 5—Continuous cycle fatigue data for AF-115.

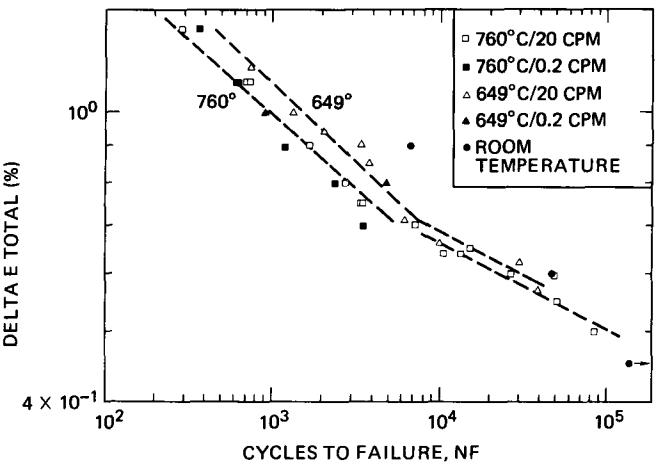

Fig. 6—Continuous cycle fatigue data for AF2-1DA.

The fatigue data for AF-115 are shown in Figure 5; fatigue life exhibits a nearly linear relationship with total strain range. This type of relationship has been predicted previously by Wells and Sullivan[9] for superalloys that deform heterogeneously. There was no appreciable effect of cyclic frequency found on fatigue life although the tests at 0.2 cpm were practically limited to the higher strain ranges (shorter lives). The best fit lines through the data also show that there was only a small effect of test temperature over the strain ranges tested.

The room temperature fatigue tests for AF-115 (as-HIP condition), although limited in number, clearly show a large increase in life compared to the elevated temperature results for the test at 0.9 pct $\Delta\varepsilon_t$. However, the scatter for these tests preclude any more definitive conclusions being drawn.

The fatigue test results for the AF2-1DA alloy are presented in Figure 6. Again, the data are represented by linear relationships with total strain range, but they now appear in two separate regimes. This representation was chosen since it not only better describes the data than a single straight line, but the change in slope can be correlated with a change in initiation mode, to be discussed in detail in the accompanying paper.[7] Figure 6 shows that there was a small reduction in life when the temperature was raised from 649 °C to 760 °C. As with AF-115, however, there was no appreciable frequency effect over the strain ranges tested. The room temperature tests also show a large increase in life at 0.9 pct $\Delta\varepsilon_t$, but again no conclusions can be drawn because of the limited number of tests.

The 760 °C, 20 cpm data for AF-115 and AF2-1DA are compared in Figure 7. The results show that in both the high and low strain range regimes, the AF2-1DA alloy had a greater fatigue life than the AF-115 alloy. These results are somewhat surprising in that it would be expected that the superalloy with the greater yield strength would exhibit superior fatigue properties when the alloys are compared at equal total strain ranges.[10,11] This result suggests that the higher defect concentration of the AF-115 alloy causes a reduction in fatigue life through its influence on crack initiation and propagation.

B. *Initiation Modes—Elevated Temperature*

SEM examination of all the elevated temperature tests showed that for both alloys there were basically two modes of initiation, one at high strain ranges and a different one at the lower strain ranges. This transition in initiation mode will be addressed in detail in the companion paper. Here, only the details of the different cracking processes will be described.

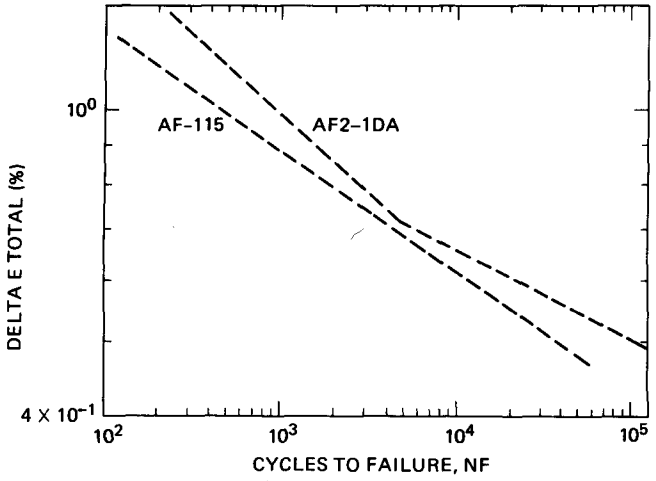

Fig. 7—Comparison of the fatigue behavior of AF-115 and AF2-1DA at 760 °C and 20 cpm.

B.1. AF-115–High $\Delta\varepsilon_t$. For AF-115 at 760 °C and 649 °C at both frequencies and at the higher strain ranges, the dominant fatigue cracks initiated at surface or near surface defects, generally preexisting argon pores. The AF-115 alloy, as previously described, had a large population of such pores. The pores that were associated with the initiation of the dominant cracks were located 10 to 20 μm below the specimen's surface, and their diameters ranged from 30 to 130 μm with the majority being between 70 and 100 μm.

An example of a pore-initiated failure is shown in Figure 8a, and at higher magnification in Figure 8b. In the latter figure the details of the cracking around the pore are apparent. Examination of the metallographic section of failed specimens showed that cracks initiated along the equator of the pore, and the cracks then propagated normal to the tensile axis in Stage II mode (Figure 9).

Initiation of the dominant crack at a near surface preexisting pore occurred in over 90 pct of the cases for AF-115 specimens fatigued at high strain ranges. There was, however, one case of initiation at a surface-connected hafnium oxide inclusion (Figure 10) and two cases of specimens that failed due to near surface initiation at other nonmetallic inclusions. These latter observations are considered to be statistically significant and related to the relative population of pores, tramp inclusions, and HfO_2 particles.

B.2. AF-115–Low $\Delta\varepsilon_t$. Below 0.7 pct total strain range, the dominant fatigue cracks in AF-115 initiated at subsurface hafnium oxide inclusions. Figure 11a shows the location on the fracture surface of one such origin, well below the specimen's surface. At higher magnification, the backscattered SEM image indicated a high concentration of the heavy element hafnium at the origin (Figure 11b).

Examination of the metallographic section of failed specimens showed secondary cracks radiating from other HfO_2 inclusions. The mode of crack initiation appears to be inclusion-matrix decohesion, with subsequent Stage II crack propagation normal to the tensile axis from the inclusion tip.

B.3. AF2-1DA–High $\Delta\varepsilon_t$. For AF2-1DA in the high strain range regime, three surface crack initiation mechanisms were observed, depending on the specific combination of cyclic frequency and temperature. These were transgranular initiation on a plane normal to the tensile axis, transgranular initiation at an angle of 45 deg to the tensile axis, and intergranular cracking.

The most prevalent mode of initiation and early growth, however, was transgranular initiation normal to the tensile direction. On the fracture surface, these sites were usually flat and featureless, as shown in Figure 12. In each case, the shape of the crack and the morphology of the tear lines indicated that the crack originated at the specimen's surface, although there was generally no obvious microstructural feature or defect on the fracture surface that could be associated with the crack origin. However, microscopic resolution in the area of the origin was limited due to oxidation and rubbing of the fracture surfaces during fatigue cycling. Serial sectioning through the cross-section of selected specimens revealed that some secondary cracks were associated with small nonmetallic inclusions (<1 μm diameter) lying near the specimen's surface (Figure 13), and others had origins near carbides that may have contributed to initiation. Thus, these Stage II cracks appear to have

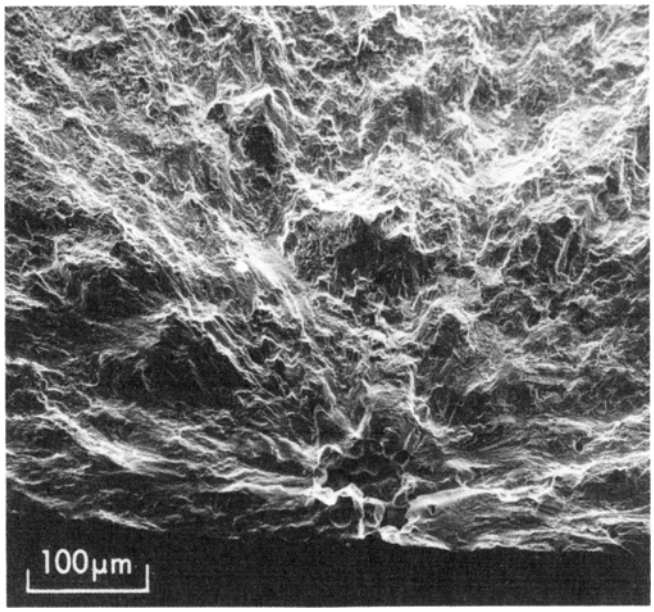

(*a*)

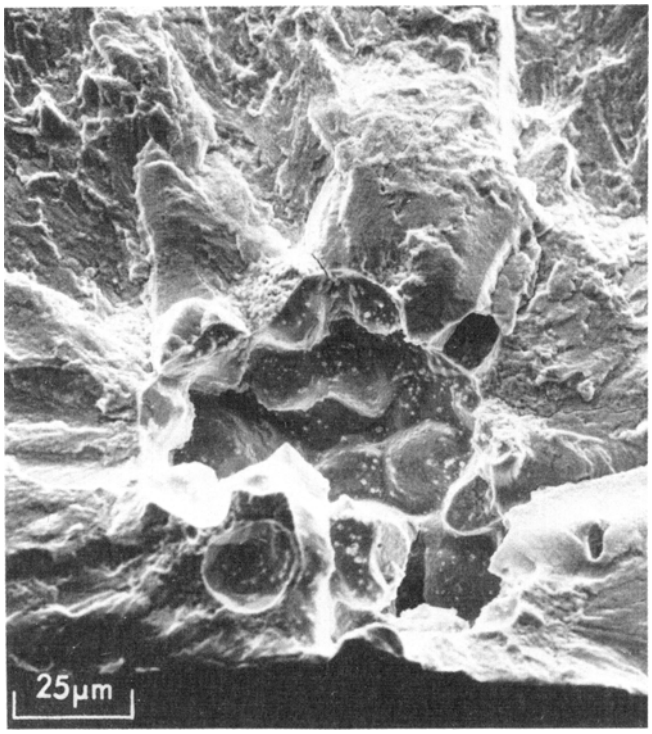

(*b*)

Fig. 8—(*a*) Fracture surface of AF-115 specimen showing failure origin at a near surface pore; (*b*) higher magnification of the same.

initiated also at defects, but in this case the defects were much smaller than the pores found in AF-115.

As discussed, two other mechanisms of surface crack initiation were observed: transgranular cracking at an angle near 45 deg to the tensile axis and intergranular initiation. The smooth, relatively featureless facets associated with the former mechanism were found on the same fracture surfaces as the Stage II initiation sites. Examination of metallographic sections revealed that in several instances these

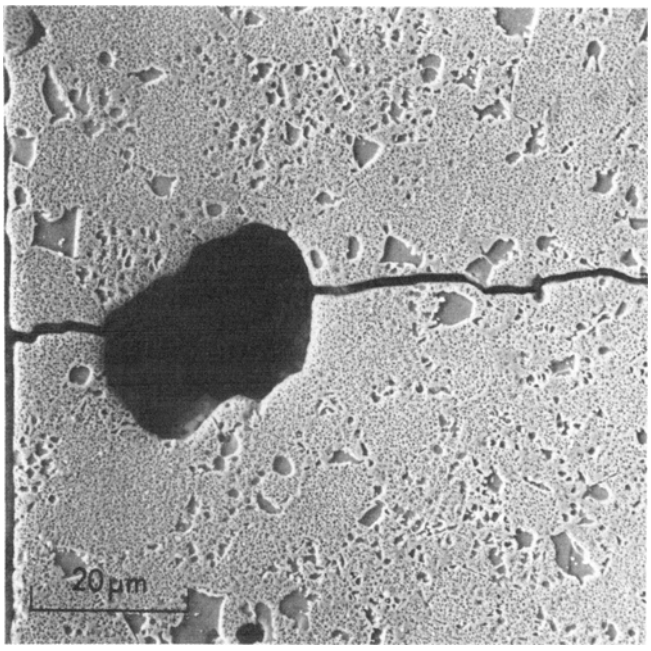

Fig. 9 — Stage II crack initiation at a near surface pore; polished and etched cross-section.

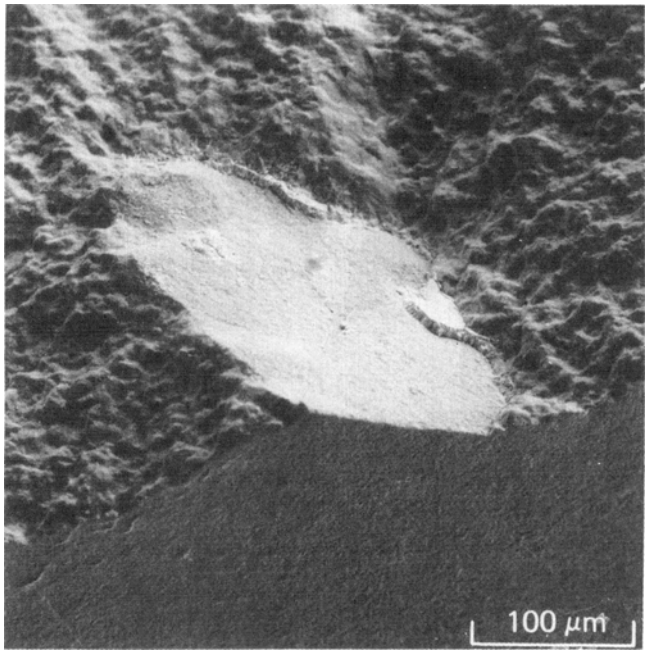

Fig. 10 — Crack initiation site at a near surface hafnium oxide inclusion on AF-115 fracture surface.

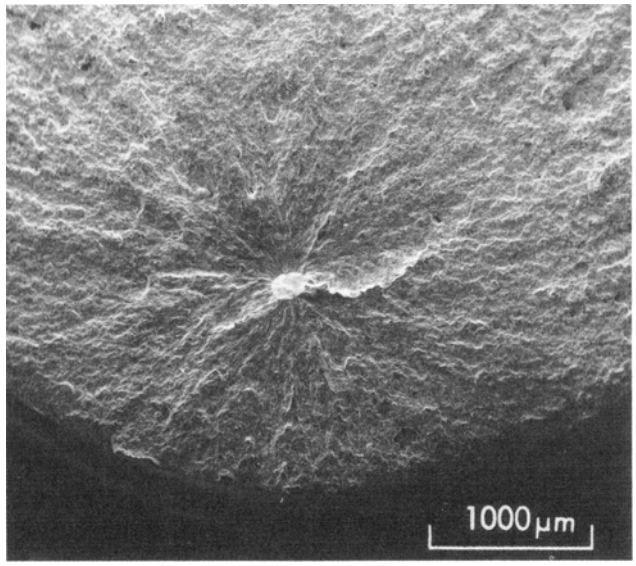

(*a*)

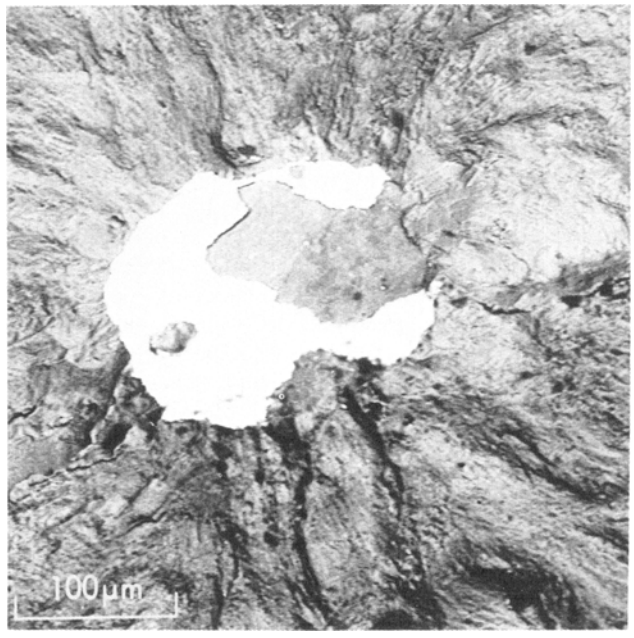

(*b*)

Fig. 11 — (*a*) Subsurface initiation site on the fracture surface of an AF-115 specimen; (*b*) SEM back scattered image of the fatigue origin.

crystallographic cracks were associated with annealing twin boundaries. Intergranular initiation occurred only at 760 °C and at the lower frequency of 0.2 cpm. As shown in Figure 14, the crack path changed from intergranular to transgranular after a small amount of growth along the boundary, so this was not a dominant mode in this investigation.

B.4. AF2-1DA – Low $\Delta\varepsilon_t$. In the lower strain range regime, the initiation site of the dominant fatigue cracks in AF2-1DA were at large nonmetallic inclusions located in the interior of the specimen. Figure 15 is a low magnification micrograph showing the origin of a fatigue failure well below the specimen surface. The origin was identified by the use of energy dispersive analysis as a stringer type inclusion rich in aluminum, magnesium, and zirconium. The mechanism of initiation at such an inclusion was generally Stage I cracking along slip bands originating at the defect, followed by Stage II crack propagation after growth of about one grain diameter.

A clearer example of this mode of cracking is shown in Figure 16; the Stage I facet which resulted from the initial stage of crack nucleation can be seen at the defect's edge

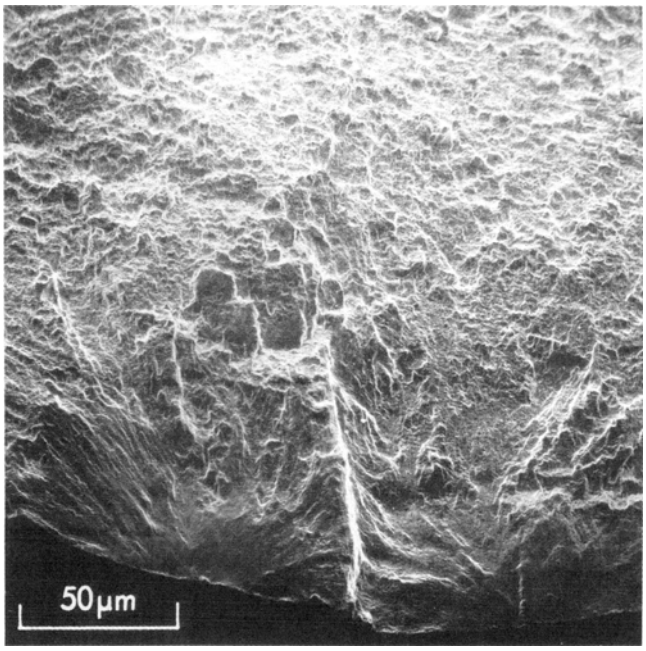

Fig. 12—SEM fractograph of a stage II surface crack initiation site in AF2-1DA.

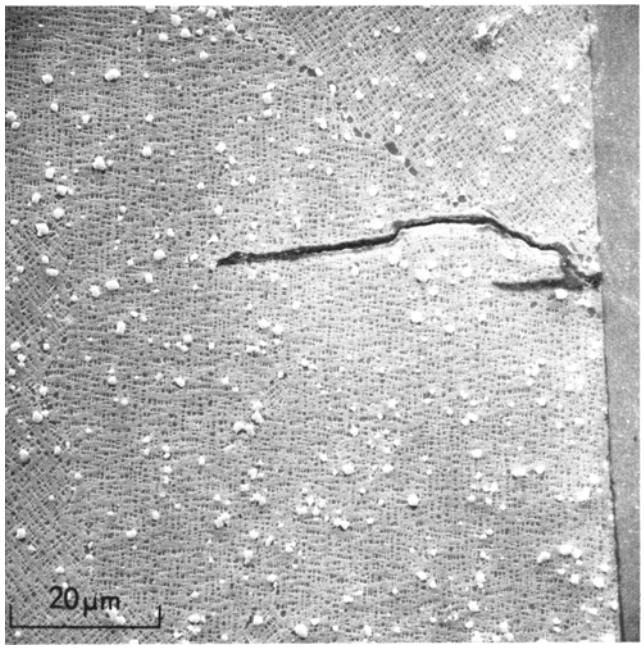

Fig. 14—Intergranular surface initiation in AF2-1DA at 760 °C and 0.2 cpm.

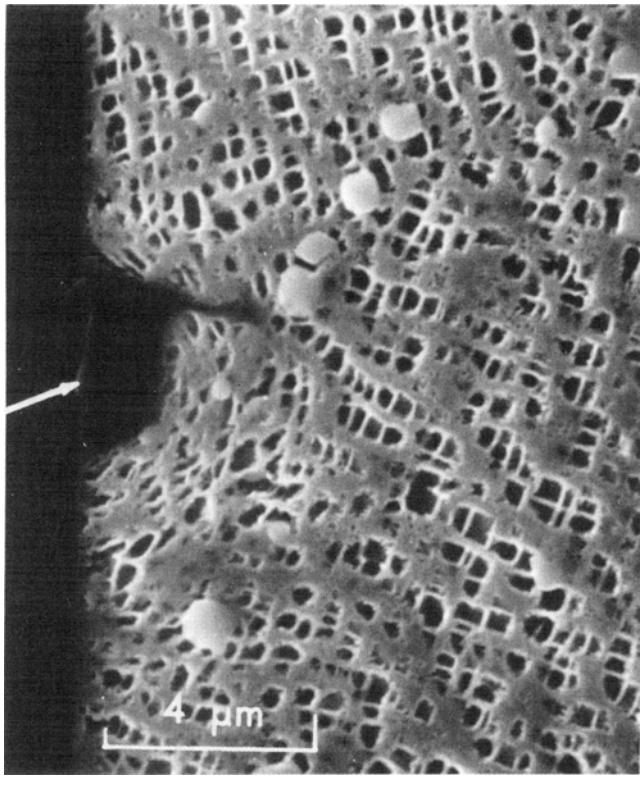

Fig. 13—Polished and etched cross-section of failed AF2-1DA specimen showing crack initiation at a small surface inclusion identified by the arrow.

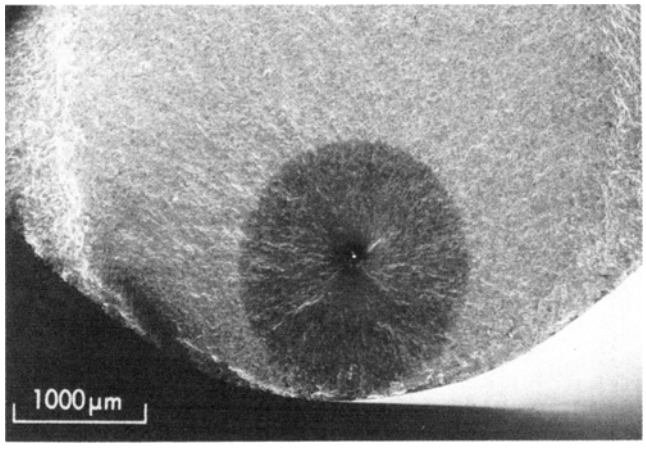

Fig. 15—Subsurface crack initiation as observed on the fracture surface of an AF2-1DA specimen.

surrounded by a fracture area typical of Stage II propagation. Examination of the metallographic section using TEM replica techniques showed Stage I shear bands at the tip of another nonmetallic inclusion (Figure 17). Initiation in this strain range regime occurred at fewer but larger defects than at higher strain ranges, and the initial mode of crack propagation was Stage I rather than Stage II.

In summary, small inclusions and carbides (~1 μm) appear to control the crack initiation process in AF2-1DA at the higher strain ranges. In the longer life tests, at low strain ranges, failure resulted from preferential cracking at large subsurface nonmetallic inclusions. In AF-115, which had a higher defect concentration than did AF2-1DA, large defects controlled the initiation process in both strain range regimes. Pores dominated the process at high $\Delta\varepsilon_t$ and the hafnium oxide inclusions were responsible for failure at lower strain ranges.

C. *Initiation Modes–Room Temperature*

To contrast with the elevated temperature results, several fatigue tests were performed at room temperature. In all

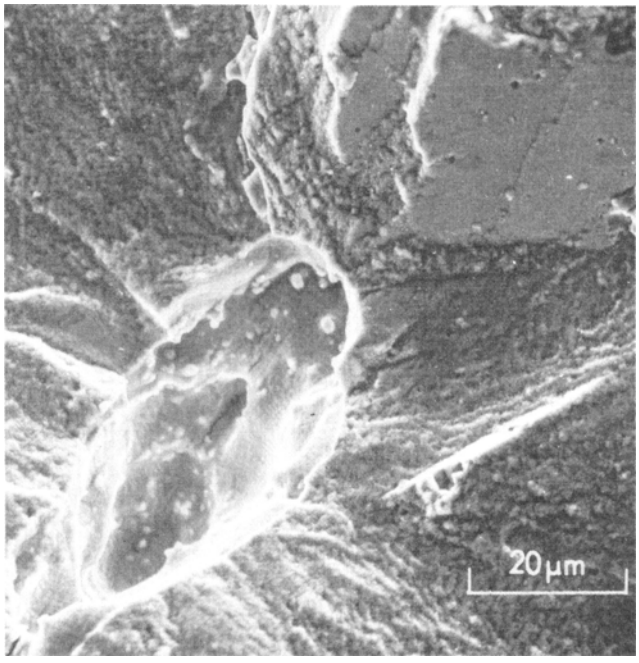

Fig. 16—Stage I facet at the edge of an internal defect as viewed on the fracture surface.

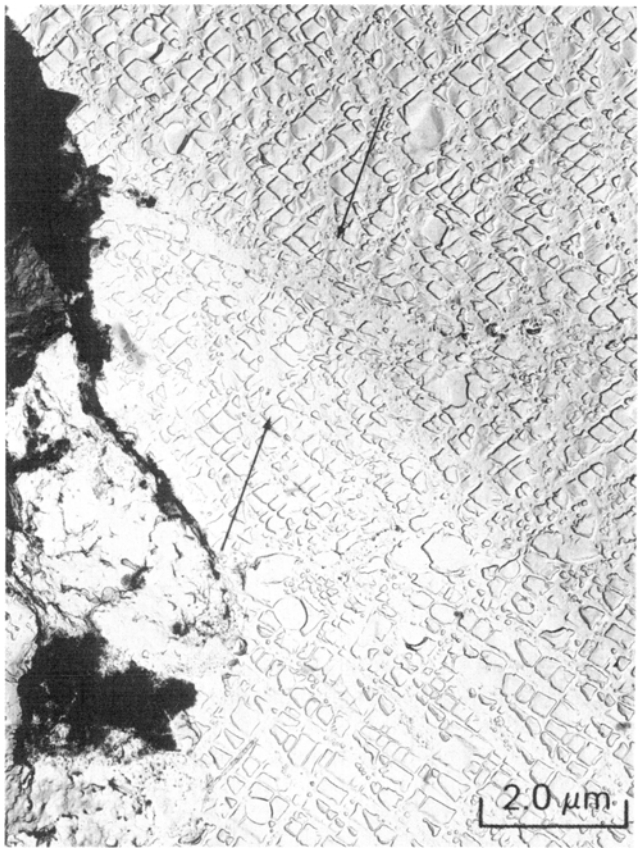

Fig. 17—TEM replica image of the Stage I initiation region adjacent to a preexisting defect. Arrows indicate parallel slip markings.

cases the initiation modes were different from those observed at elevated temperature. More importantly, there was no longer a difference in initiation mode over the strain ranges tested. Thin foil TEM analysis was performed to help rationalize these differences.

AF2-1DA specimens were tested at room temperature at total strain ranges of 0.9 pct, 0.6 pct, and 0.4 pct. For the first two tests, initiation occurred by surface cracking along intense planar slip bands at approximately 45 deg to the tensile axis. The test at 0.4 pct $\Delta\varepsilon_t$ was terminated at 5×10^6 cycles without failure; no detectable cracking was observed on the specimen's surface.

Figure 18a shows a central region of the polished and etched cross-section of the failed AF2-1DA specimen tested at 0.9 pct $\Delta\varepsilon_t$; evidence of intense planar slip was present in all grains throughout the specimen. Within the surface

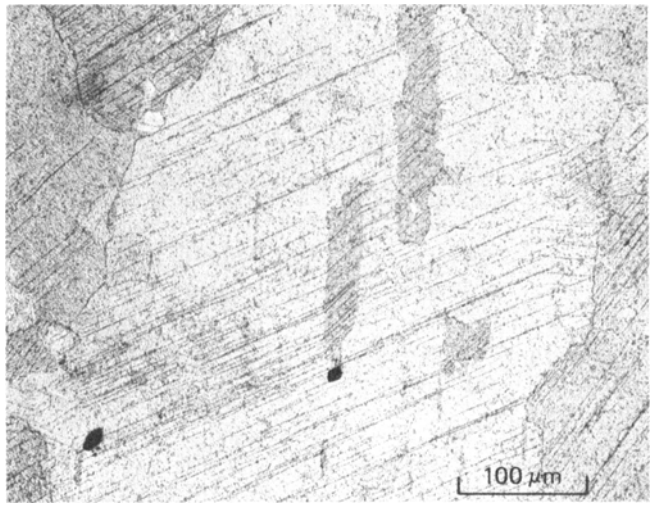

(*a*)

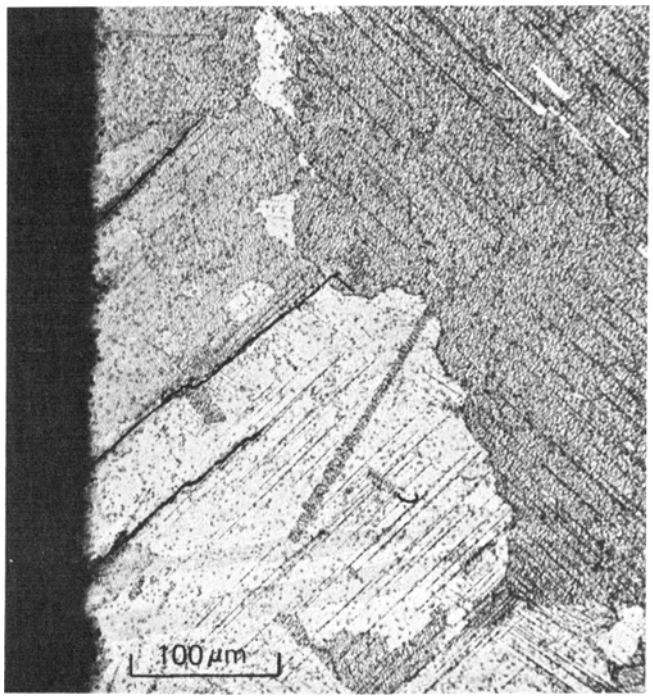

(*b*)

Fig. 18—Optical micrographs showing (*a*) the intense planar slip in the central portion of a room temperature fatigue specimen; (*b*) Stage I cracking at specimen's surface (cross-sectional view).

grains, parallel cracks formed along the slip bands in a Stage I mode as shown in Figure 18b. Evidence of Stage I initiation was also present on the fracture surfaces of the 0.9 pct $\Delta\varepsilon_t$ test where crystallographic facets were observed at the origin of the dominant crack.

The specimen fatigued at 0.6 pct $\Delta\varepsilon_t$ had similar Stage I facets on the fracture surfaces. The degree of intense planar deformation observed on the metallurgical sections was, however, considerably reduced. In fact, slip traces were not observed throughout the specimen cross-section, but were confined to a few surface or near-surface grains. As at the higher strain ranges, there was no apparent defect associated with the initiation of the surface Stage I cracks.

Three fatigue tests were performed on AF-115 at room temperature; the cyclic strain ranges were 0.9 pct, 0.6 pct, and 0.44 pct. In all cases the dominant fatigue cracks initiated along planar slip bands adjacent to a near-surface pore. On the fracture surface, crystallographic cracking was evident around those pores which were the fatigue origins (Figure 19). At higher magnification, the Stage I planes appeared similar to cleavage facets as in AF2-1DA. Metallographic sections revealed further details of the Stage I initiation process. Figure 20a shows a near-surface pore with cracks emanating along planes of maximum shear strain at an angle of approximately 45 deg to the tensile axis. TEM replica examination of this pore showed intense slip traces parallel to the main crack (Figure 20b), as evidenced by cutting of the γ' precipitates.

At room temperature, crack initiation in both alloys occurred at the surface or at near-surface defects as in the high strain range elevated temperature tests. However, the initiation mode was considerably different, being Stage I crystallographic cracking as opposed to the Stage II mode of cracking found predominantly at the high temperatures. Previously such changes in initiation mode with temperature have been attributed to changes in deformation behavior,[12,13]

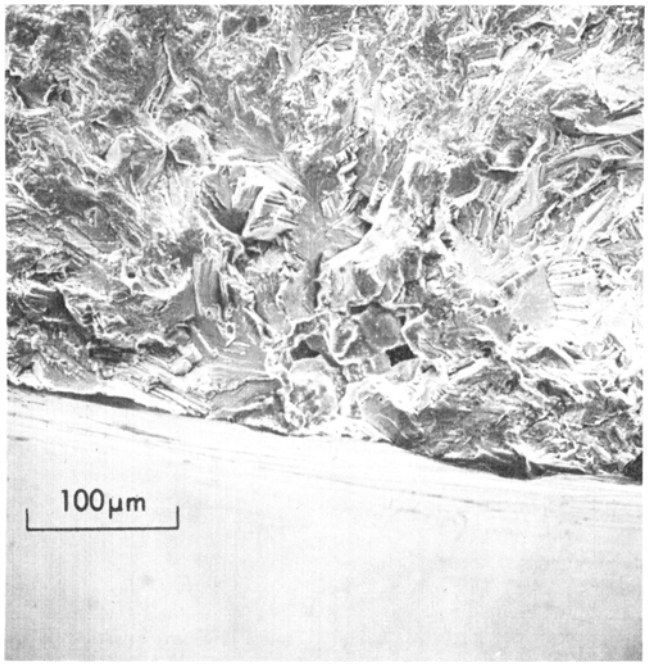

Fig. 19—Stage I cracking in AF-115 at room temperature originating at a near surface pore.

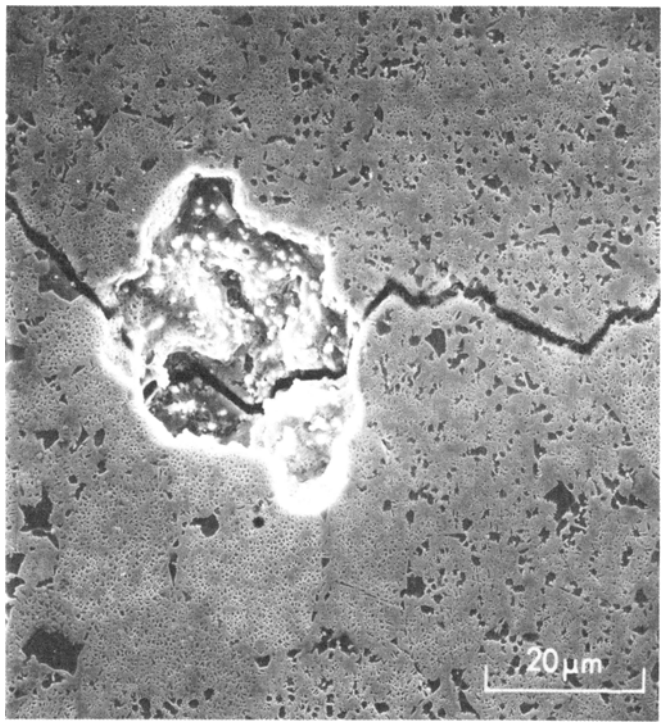

(*a*)

(*b*)

Fig. 20—(*a*) Cross sectional view of a Stage I crack originating at a near surface pore in AF-115; (*b*) TEM replica image of the cracked region between the pore and the surface edge in the accompanying micrograph showing planar slip bands parallel to the Stage I crack.

although it has also been suggested that surface oxidation may also play an important role.[14] Nickel-base superalloys generally deform in a planar and heterogeneous slip mode at room temperature, and with increasing temperature the slip becomes more homogeneous and wavy.[12,13] This was observed in limited thin foil microscopy performed in this study. Figure 21a shows an example of the planar type of deformation exhibited by AF2-1DA fatigued at room temperature at 1.1 pct $\Delta\varepsilon_t$. This intense localization of deformation into parallel slip bands for alloys with ordered precipitates, such as the nickel-base superalloys, has been related to localized softening of the slip band due to shear of the ordered precipitates.[15–18] The resultant strain localization leads to cracking in the slip band. At the same strain range, 1.1 pct, the deformation at 760 °C was much more homogeneous and wavy, as shown in Figure 21b. This deformation accumulates especially near discontinuities and strain concentrators, and Stage II initiation results. This process has been described as cracking on alternating slip planes.[19]

In summary, this study has shown the significant role defects play in the initiation process. Large internal defects were the initiation sites for both alloys at low strain ranges, while smaller, more populous defects controlled the failure process at higher strain ranges. This relationship is addressed in the subsequent paper.

V. CONCLUSIONS

1. For the high strength P/M nickel-base superalloys, AF2-1DA and AF-115, a change in the elevated temperature initiation mode of the dominant crack that caused failure was observed as the strain range was changed: at higher strain ranges initiation was at or near the specimen's surface, while at the lower strain ranges the failure site was in the specimen interior.
2. At elevated temperature, smaller, more populous defects such as pores controlled the initiation process at the higher strain ranges. At the lower strain ranges, the cracks that caused failure initiated at the larger nonmetallic inclusions. Cracking at elevated temperature occurred in both Stage I and Stage II modes, depending on the alloy and the strain range.
3. For both alloys, the initiation mode at room temperature was different than at elevated temperature. Dominant cracks initiated at or near the surface; there were no internal failure origins. Stage I crystallographic cracking dominated the initiation process in this regime.

ACKNOWLEDGMENTS

The authors would like to thank Professors J. C. Williams, A. W. Thompson, and J. L. Swedlow of Carnegie-Mellon University for valuable discussions. JMH also gratefully acknowledges technical discussions with Dr. G. R. Leverant of SWRI and the support of Dr. W. H. Reimann and Dr. T. Nicholas of the Air Force Materials Laboratory. This research was performed while JMH was Metallurgist, Air Force Materials Laboratory, Wright Aeronautical Laboratories, Wright-Patterson AFB, Ohio, and was part of AFML inhouse project 2307P102.

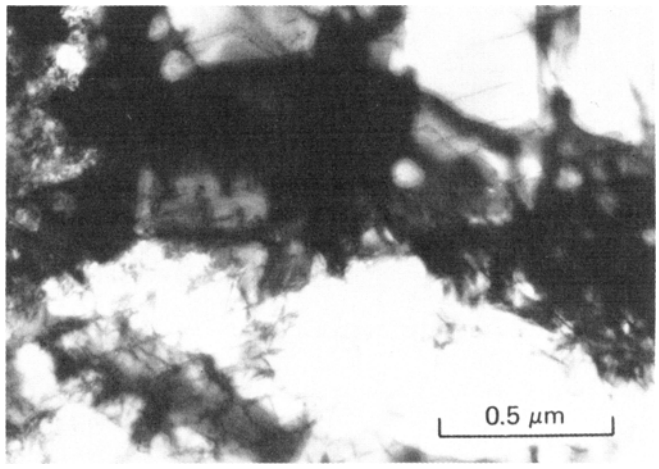

(*a*)

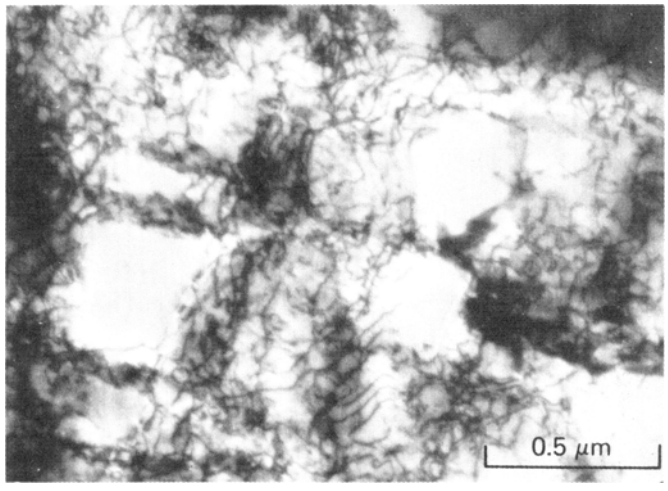

(*b*)

Fig. 21—(*a*) Planar slip character of room temperature deformation in AF2-1DA at 1.1 pct $\Delta\varepsilon_t$; (*b*) wavy slip character of elevated temperature deformation in AF2-1DA at 1.1 pct $\Delta\varepsilon_t$.

REFERENCES

1. F. de Kazinczy: *JISI*, 1970, vol. 207, p. 851.
2. M. Gell and G. R. Leverant: *Trans. TMS-AIME*, 1968, vol. 242, p. 1869.
3. J. C. Grosskreutz and G. G. Shaw: *Fracture*, Second International Conf. Fracture, Brighton, P. L. Pratt, ed., Chapman and Hall LTD, London, 1969, p. 620.
4. J. Lankford: *International Metals Review*, 1977, vol. 22, p. 221.
5. M. Gell and G. R. Leverant: *Fatigue at Elevated Temperature*, ASTM STP, Am. Soc. Testing and Mat'ls, 1973, vol. 520, p. 37.
6. J. C. Grosskreutz: *Metal Fatigue Damage*, S. S. Manson, ed., ASTM STP, Am. Soc. Testing and Mat'ls, 1971, vol. 495, p. 3.
7. J. M. Hyzak and I. M. Bernstein: *Metall. Trans. A*, 1982, vol. 13A, pp. 45-52
8. J. M. Hyzak: "The Effect of Defects on the Fatigue Crack Initiation Process in Two P/M Superalloys," AFML-TR-80-4063, Air Force Materials Laboratory, Wright-Patterson AFB, Ohio, 1980.
9. C. H. Wells and C. P. Sullivan: *Trans. ASM*, 1968, vol. 61, p. 149.
10. B. A. Cowles, D. L. Sims, and J. R. Warren: "Evaluation of the Cycle Behavior of Aircraft Turbine Disk Alloys," NASA Report CR159409, 1978.
11. V. Shahani and H. G. Popp: "Evaluation of the Cyclic Behavior of Aircraft Turbine Disk Alloys," NASA Report CR-159433, 1978.
12. M. Gell and G. R. Leverant: *Ordered Alloys*, Third Bolton Landing

Conf., AIME, Claitor's Publishing, Baton Rouge, 1970, p. 505.
13. J. M. Oblak and B. H. Kear: *Electron Microscopy and Structure of Materials*, Univ. of California Press, Berkeley, 1972, p. 566.
14. L. F. Coffin, Jr.: *Fatigue at Elevated Temperature*, ASTM STP, Am. Soc. Testing and Mat'ls, 1973, vol. 520, p. 5.
15. C. Calabrese and C. Laird: *Matl. Sci. and Engr.*, 1974, vol. 13, p. 141.
16. C. Calabrese and C. Laird: *Matl. Sci. and Engr.*, 1974, vol. 13, p. 159.
17. C. Calabrese and C. Laird: *Metall. Trans.*, 1974, vol. 5, p. 1785.
18. R. E. Stoltz and A. G. Pineau: *Matl. Sci. and Engr.*, 1978, vol. 34, p. 275.
19. C. Laird: *Fatigue Crack Propagation*, ASTM STP, Am. Soc. Testing and Mat'ls, 1967, vol. 520, p. 131.
20. C. Laird and D. J. Duquette: *Corrosion Fatigue*, NACE-2, 1972, p. 88.